UNSYS digital

Journal of Unmanned System Technology

Design and Analysis of Modular, Portable, Rapid Deployment Autonomous Surveillance UAV System

Imron Anshori[†], Sufendi[†], Luqman Haris[†], Pepi Saepudin[†], Aris Budiyarto[†], Agus Budiyono[‡]

[†]Bhimasena Research and Technology, Sumedang, Indonesia

[‡]Department of Aerospace and Aviation, RMIT University, Melbourne, Australia

Abstract—In open field operations, such as in the isolated mountainous area, the need of small, compact, and portable surveillance system is inevitable [7]. It is to give the team a surveillance capability while reducing carried-load significantly. This system is a portable mini unmanned aerial vehicle (UAV) with its mobile Ground Control Systems included. Within this paper, the general design processes are presented from determining DRO, initial sizing, aerodynamics analysis, structure, mechanism, backpack design until flight testing to validate the design. Some simple simulations by XFLR5 and complex simulation CFD are also conducted to predict the aerodynamics characteristic of UAV. Outdoor flight testing has been conducted and also still on progress for further results.

Keywords—Backpack UAV, modular, mobile surveillance.

I. Introduction

For the purpose of expedition, mapping on a new area or in combat situation, a team with several members in it sometimes performs their operation within a few weeks inside various terrains combination and change, such as tropical forest, savanna, desert, mountain and hills. Such those harsh environments, the amount of logistic and survival tools the team can carry is very limited. In addition of support equipment, it will reduce the performance of whole team. While at the same time, the demands of a mobile surveillance/mapping system which fully supports the scout capability desperately become a critical issue. The UAV system must have flexibility to maintain the performance of whole team while moving or in critical situation. So the keys of the design are compact, modular, lightweight, rapid deployment, and scout-function ability.

II. Design Requirements and Objectives

In present work, the boundaries are given by DRO as it shown in **Table I**.

III. Comparative Study

Before determining the detailed configuration, it needs to study other competitor's UAV. Three choices are chosen to get the big picture of what will be designed, as presented in **Table II**.

Corresponding author: Agus Budiyono (e-mail: agus.budiyono@rmit.edu.au)
This paper was submitted on November 13, 2013; revised on August 7, 2014; and accepted on December 27, 2015.
DOI: 10.21535/just.v3i3.751

Table I DRO

Specification	DRO
Type	Fixed wing
Operator	1 personnel
Deployment time	No more than 2 minutes
Take off method	Hand launch / catapult chord
Landing method	Belly landing / net
Carrier / packing	Backpack
Flight mode	Manual, semi, fully autonomous
Top. Speed	110 km/h
Cruise speed	60 km/h
Operating altitude	60-200 m (AGL)
Endurance time	Up to 60 minutes
MTOW	1.6 kg
Wingspan	1.3 m
Other features	Swappable two different cameras
	Shock & impact proof

Table II Comparison of Specifications

Specifications	Raven[4]	eBee	Wasp AE[5]
Configuration	Tail boom	Flying wing	Tail boom
Weight (kg)	1.9	0.7	1.3
Wingspan (cm)	140	96	102
Endurance (min)	60-110	50	50
Range (km)	10	3	5
Top speed (km/h)	81	90	83
camera	EO & IR	EO	IR & EO
launching	Hand launch	Hand launch	Hand launch
landing	Deep stall / belly	Belly	Deep stall
Image			

Tail boom UAV gets better endurance because it can do slow flight and heavy battery or more payloads mounted inside. But it lacks on top speed and more drag produced than flying wing configuration. Besides, it has more parts to assemble and disassemble, and then more time will be consumed.

To achieve rapid deployment by getting UAV ready less than two minutes, flying wing configuration is chosen. In this configuration too, modular and portable can be easier to be designed. The initial brainstorming phase shows that it requires fuselage to hold before throwing and vertical tails or winglet to stabilize in lateral plane.

IV. Weight Estimation

An estimation of overall weight will be calculated before initial sizing as an input for geometric definition later. The weight of components can be divided into four main categories: airframes, propulsion, electronics, and payload.

Airframes included wings, spars, fuselage, tails, battery case, autopilot case, mounting and other structures. They are almost all produced in composite material. Propulsion included battery, propeller, ESC, and motor. Payload only consists of camera and its connector because it's the only one that requires switching for different kind of mission. For other electronics it includes video sender, telemetry transmitter, servos, GPS, voltage regulator, autopilot, R/C receiver and other connectors or cables. The total weight is targeted to be up to 1.54 kg. The distribution can be seen in **Figure 1**.

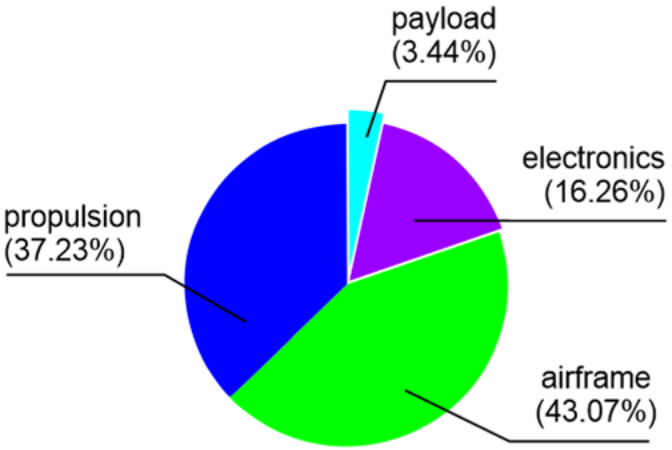

Figure 1 Pie chart of weight distribution

V. Initial Sizing

The assumption of air density for initial sizing is 1.14 kg/m^3 because the mountainous area is mostly not at near sea level. The gravitational force is 9.81 m/s^2. For easy take-off and landing, the wing loading must be between 4-5 kg/m^2. For the stability, the position of CoG-Neutral point compared to MAC of wings should be around 5% [3]. But in the present work, this number exceeds until 8.97%, too stable. The overview of initial sizing phase can be seen on **Table III**.

Table III Initial sizing parameters

Group	Parameter	Value	Unit
Overall	NP	0.27	m
	CG X	0.25	m
	CG Z	0.01	m
	σ	8.97	%
	C_L Designed	0.09 – 0.57	-
Wing	Span	1.30	m
	Root chord	0.28	m
	Tip chord	0.18	m
	Aspect ratio	5.65	-
	Taper ratio	0.64	-
	Mac	0.230	m
	Area	0.29	m^2
	Wing load.	5.15	kg/m^2
	Twist	0	degree
	Dihedral	0	degree
	Sweep 0.25	19.5	degree
	Sweep LE	21.6	degree
	Incident	0	degree
	Xw	0.10	m
	Zw	0.03	m
Twin vertical tails	Span	0.13	m
	Root chord	0.125	m
	Tip chord	0.075	m
	Sweep 0.25	29	degree
	Sweep LE	33	degree
	MAC	0.1	m
	xv	0.43	m
	yv	0.14	m
	zv	0.024	m
	Area (each)	0.013	m^2
	Aspect Ratio	1.3	-
	Taper ratio	0.6	-
Body	Length	0.42	m
	Diameter	0.1	m

The configuration for wing mounting is *high wing*, which gives stability in roll axis. Like eBee, it needs twin vertical tails to gives balance and stability in yaw axis. Wing swept gives *Neutral Point* further backward, so it makes easier for arrangement of components.

VI. Aerodynamics Analysis

A. Airfoil Selection

Low Reynold number airfoils from Eppler family are chosen as candidates for flying wing configuration. Because it is tailless, E186 is chosen as the final choice for better pitching moment over drag as presented in **Figure 2** below.

B. XFLR5

It is free open source software, developed and distributed under GNU General Public Licensed [5]. It has XFoil engine and ability to quickly run simple 3D model of aircraft based on wing and other surface area. After parameters of initial sizing have been defined in the previous section and airfoil has been chosen, they put together into XFLR5 to be analyzed in a complete configuration but simple process based on Lifting Line Theory, as shown in **Figure 3**. Other methods are available, such as Ring vortex and Horseshoe vortex.

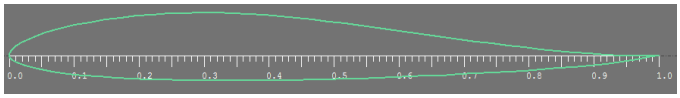

Figure 2 Eppler E186 airfoil

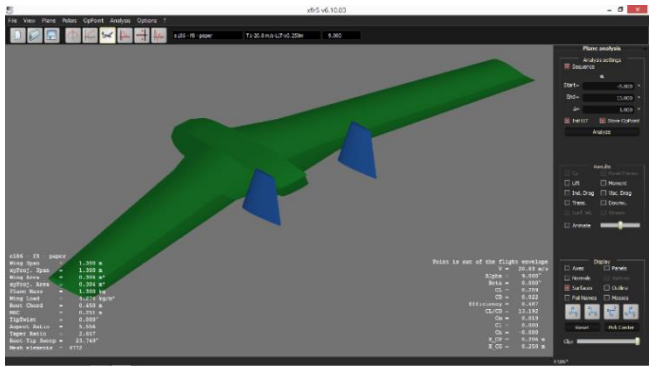

Figure 3 UAV model in XFLR5 in full configuration

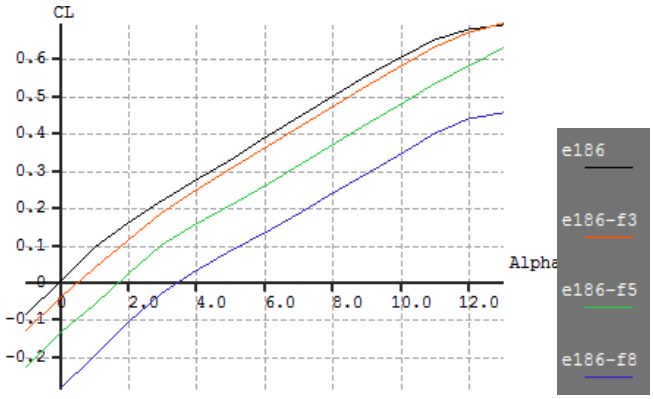

Figure 4 C_L vs AoA

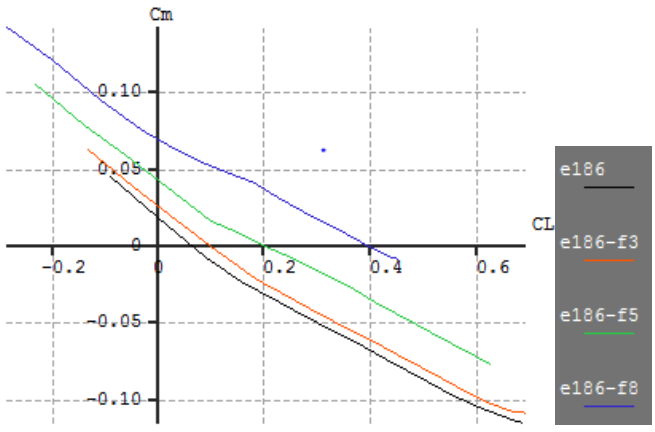

Figure 5 C_m vs C_L

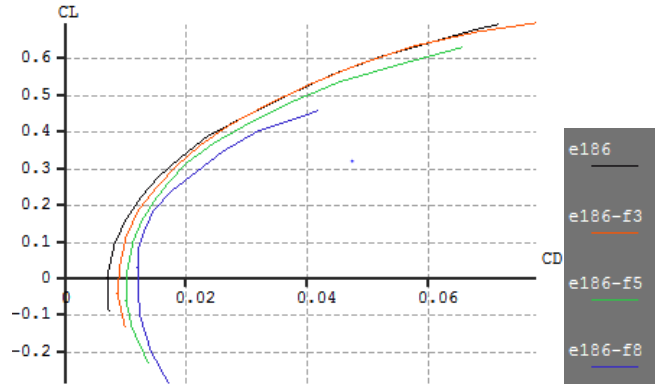

Figure 6 C_L vs C_D

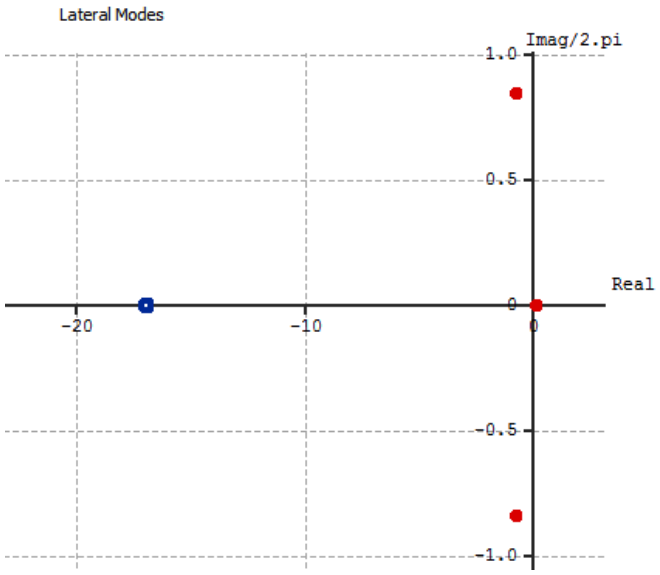

Figure 7 Root locus view in lateral mode

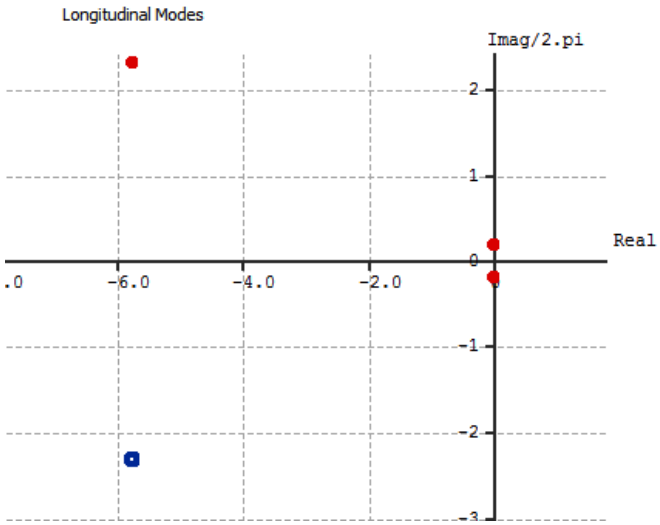

Figure 8 Root locus view in longitudinal mode

The model has two ailerons deflected on left and right of the wings symmetrically by the number three, five and eight degrees. The results of lift coefficient vs angle of attack (AoA), moment coefficient vs lift coefficient, and polar drag are presented in **Figure 4**, **Figure 5**, and **Figure 6**.

Figure 5 shows that the minimum value of C_L can be obtained up to 0.4 at zero pitching moment when elevon deflection is eight degree. It still can be increased to achieve bigger C_L value when needed.

Another result from XFLR5 is root locus view describing its stability characteristics of dynamics motion, as in **Figure 7** and **Figure 8**. In **Figure 7**, it has two symmetric dutch roll modes, one roll damping mode and one spiral mode.

While in **Figure 8**, it has symmetric two phugoid modes, and two symmetric short period modes. Based on two provided root locus views above, the UAV can be said to be stable in both longitudinal mode and lateral mode.

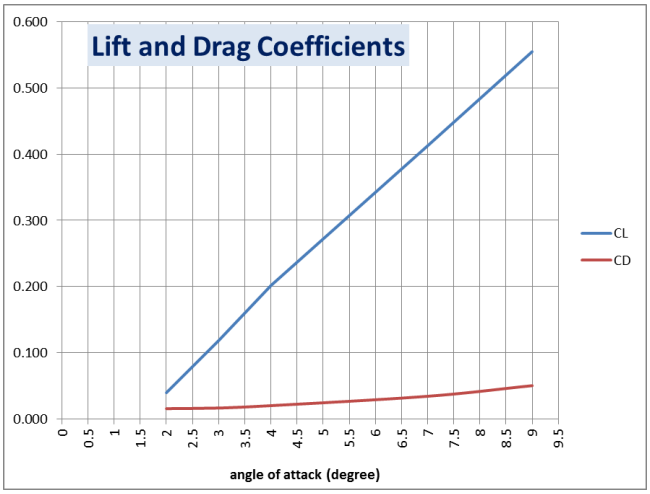

Figure 9 Lift & drag coefficient vs AoA

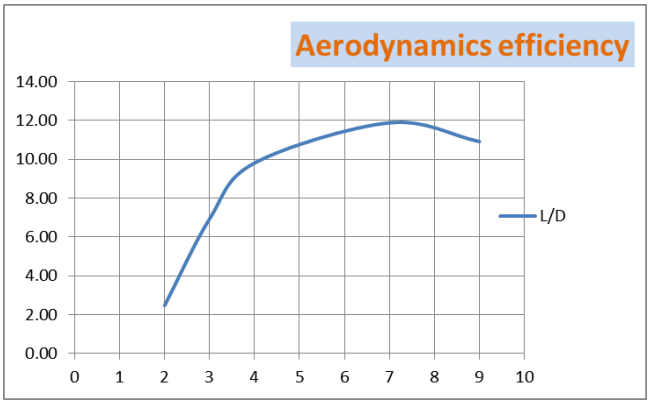

Figure 10 Aerodynamic efficiency (L/D) vs AoA

C. Ansys CFX

To make deeper analysis about the prediction of real drag, analysis of Ansys CFX has been carried out.

The 3D geometry step file is imported to ICEM CFD to be meshed using unstructured mesh. In CFX-Pre, boundaries are defined with its respective properties such as inlet, outlet, far field, wall and symmetry. In CFX-solver manager the calculation takes place, and the last is CFD-Post to analyze and get the detailed numbers of forces and moments. The raw numbers of forces and moments are converted to coefficient of lift and drag, creating lift and drag chart as shown in **Figure 9** and aerodynamic efficiency in **Figure 10**.

As compared between blue curve in **Figure 9** and black curve in **Figure 4**, the difference between XFLR5 and Ansys CFX only gives 1.5 degree drifted-curve to the right. For the drag, Ansys CFX gives slightly bigger values than XFLR5. From **Figure 10**, maximum L/D is obtained at AoA of 7 degree. This would be an ideal attitude for cruise mode, for the longest endurance that is possible to achieve.

VII. Motor Selection

For estimation of thrust, an equation **(1)** from [2] gives some accurate output of thrust from inputs of RPM, propeller diameter and pitch.

$$F = 1.225\frac{\pi(0.0254\cdot d)^2}{4}\left[\left(RPM_{prop}\cdot 0.0254\cdot pitch\cdot\frac{1min}{60sec}\right)^2 - \left(RPM_{prop}\cdot 0.0254\cdot pitch\cdot\frac{1min}{60sec}\right)V_0\right]\left(\frac{d}{3.29546\cdot pitch}\right)^{1.5} \quad (1)$$

The configuration of the propulsion system tested is 3S LiPo 8000 mA·h 11.1V, ESC 40A, brushless motor 2836-1600KV, and TGS sport 8x6E propeller. For whole configuration of propulsion at static thrust test, it gives 1.2 kg force static thrust at 13800 rpm.

Although the RPM dynamically increases through increasing airspeed, this assumption of static rpm then become the input of equation to get estimation of maximum velocity of UAV as shown in **Figure 11**. The drag curves are obtained from Ansys CFD and XFLR5 data. The orange curved indicates that rpm should be revved higher into some value to meet the targeted DRO speed.

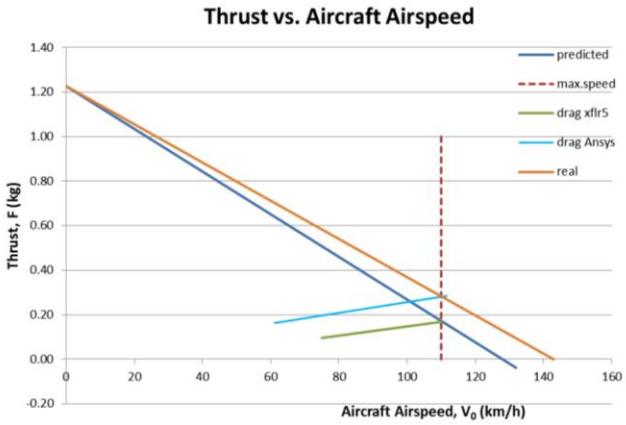

Figure 11 Thrust vs airspeed

VIII. Structures and Mechanisms

To meet the requirement of mobility and portability, the parts of UAV should be able to be disassembled and be put into a backpack. The UAV itself has been designed to be broken down easily to several parts (**Figure 12**). Whenever it needs to be deployed in some area, it should only takes less than two minutes to set it up. So, some structures and mechanisms have been designed to hasten up the deployment and packing.

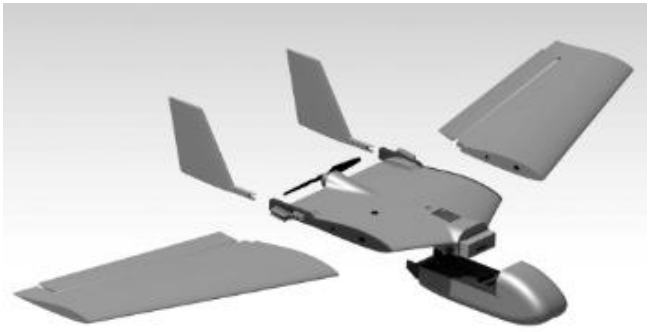

Figure 12 Assembly Parts of UAV

A. *Wing to main fuselage joint*

Instead of mechanical lock, wing joint to main fuselage has been replaced by three pairs of magnetic lock to provide quick lock. Each pair of magnet can hold up to 380 grams of load. Two spars are made of wood on each wing. If somehow the wing hits ground or whatever harshly, these spars hopefully would be broken first.

B. *Lower fuselage to main fuselage joint*

The biggest load occurs between both when bungee cord or hand launch is used to launch the UAV during take-off. Mechanical lock is used to provide greater strength up to its structural strength. In **Figure 13**, the hook shaped in darker color with its mounting to the other side is joined together with the vicinity of composite structure.

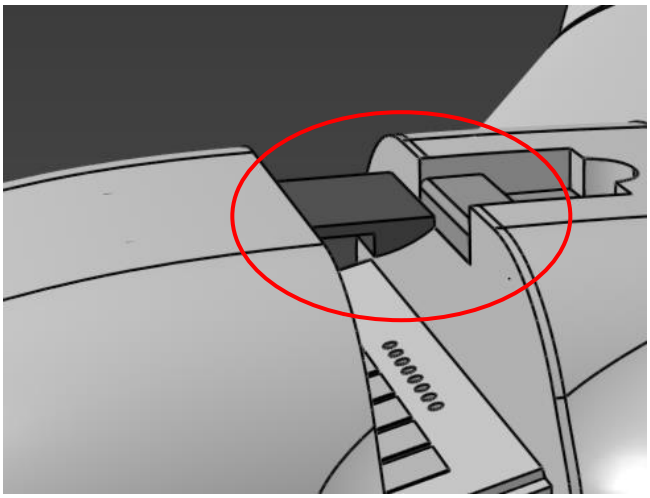

Figure 13 Lower to main fuselage joint

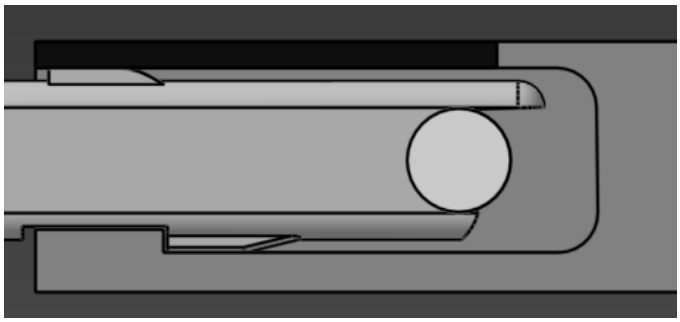

Figure 14 Vertical tail to main fuselage rib

C. *Vertical tails to main fuselage rib joint*

In **Figure 14**, the vertical tail is attached to small rounded structure inside rib and still can rotate about it for small angle. The structure that is a hook shaped has function to hold vertical tail to stay in its position while moving. When it strikes ground when hard landing occurs, it deflected up and the black plate on top freely opens. Sometimes, it can leave its initial position, get disassembled to avoid fracture.

IX. Launch Analysis

Because it has no big launcher to carry, the choice left is only throwing by hand or by bungee cord catapult. It is when critical phase occurs, whether it successfully takes off or falls over the ground because of insufficient speed to create enough lift. This analysis comes up with two-dimensional equations about horizontal axis and vertical axis. Thrust and drag are involved in horizontal axis as function of horizontal velocity, giving the equation:

$$T_{(v)} - D_{(v)} = ma_{(t)_x} \tag{2}$$

$$a_{(t)_x} = \frac{T_{(v)} - 0.5\rho {V_{(t)}}^2 S C_D}{m} \tag{3}$$

$T_{(v)}$ is the thrust as function of velocity as in equation **(1)**. Lift and weight are involved in vertical axis dynamic movement.

$$L - mg = m \cdot a_{(t)_y} \tag{4}$$

$$a_{(t)_y} = \frac{0.5\rho {V_{(t)}}^2 S C_L}{m} - g \tag{5}$$

And for both horizontal and vertical axis, governing equation for velocity and displacement are

$$V_{(t)} = V_o + a_{(t)}t \tag{6}$$

$$x_t = V_{(t)}t + 0.5a_t t^2 \tag{7}$$

Initial velocity V_o can be from hand launch speed or bungee cord pull speed. It is up to 11 m/s for normal person and the angle of throwing can vary from 9 degree to 17 degree. Finally 2D takeoff path can be estimated from equations **(2)-(7)** and some governing parameters, as one of the results is shown in **Figure 15** for partial condition. The formulation above can be used to estimate the launch from bungee cord or catapult as the alternative of throwing by hand.

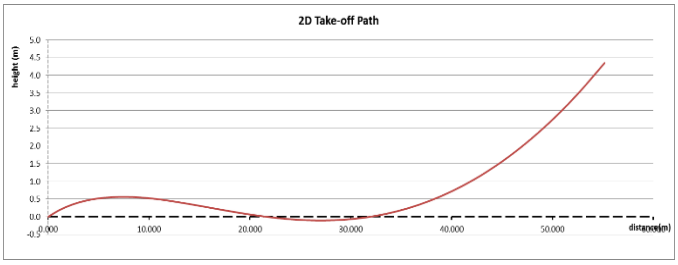

Figure 15 Two-dimensional take-off path

X. Design of Backpack

Backpack is the medium to carry all parts of UAV and all ground control station (GCS) equipment. It also protects anything inside while carrying or transporting. So it has to be hard-shell made and rainproof (**Figure 16**). This hard-shell is made from carbon fiber composite and ABS plastic. The key feature of the backpack is the accessibility to load or unload the contents inside rapidly. The smart compartment has been redesigned into three main parts (**Figure 17**); compartment 1 for the airframes, separator for wings and vertical tails, and compartment 2 for the ground control station, GCS.

Based on many tests conducted for the deployment, unloading and assembly process of the UAV takes less than two minutes, but the booting process of OS inside laptop and autorun process of the mission planning software takes more than two minutes in reality. So the booting process should be optimized to achieve more efficient time.

Figure 16 Hard-shell and rainproof design of backpack

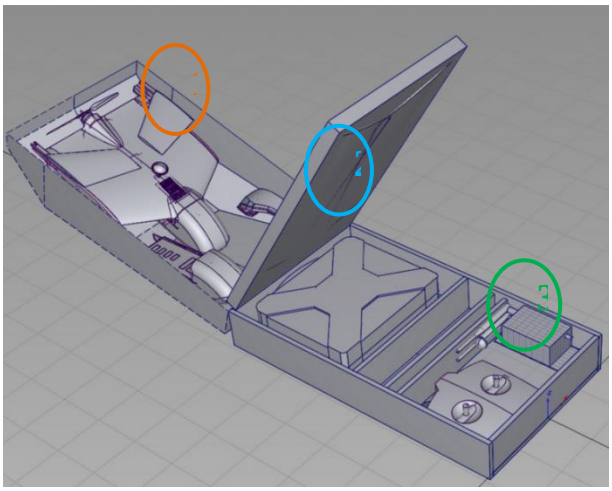

Figure 17 three main parts of backpack

Figure 18 Flight test at Cipatat, Bandung

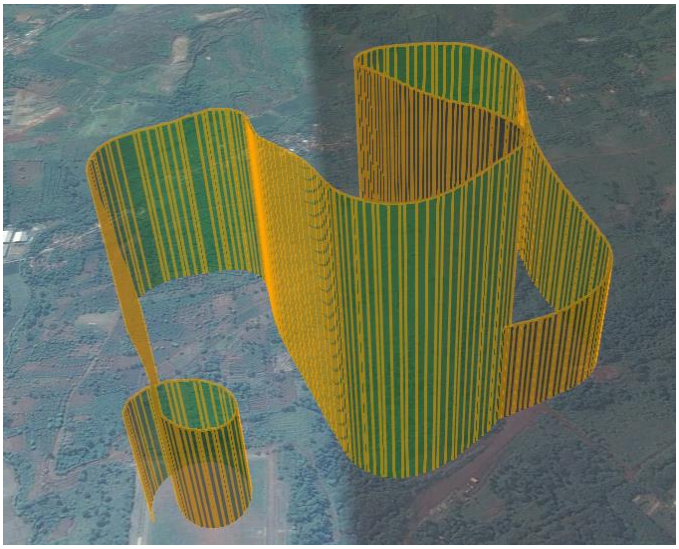

Figure 19 One of flight path extracted from telemetry log and displayed in Google Earth

XI. Flight Tests

Some flight test sites in Bandung are at Cipatat (**Figure 18**), Sulaiman Airport, and Suparlan Airport, Batujajar.

Several flight tests have been conducted on those area and some results of performance have been out based on telemetry data log as stated bellow.

- The maximum airspeed measured is 109 km/h (estimation based on IMU and GPS)
- Climb rate is up to 200 m / minute
- Stall speed approximately 45 km/h for 1.63 kg take-off weight
- Maximum height above ground that can be reached is 408 meters (from altitude 425 ASL).
- Longest flight time is 23 minutes nonstop in various flight modes, from 11.9 Volts until 10.84 Volts. But in autonomous mode, it can fly 22 minutes nonstop, from 12.3 Volts until 11.4 Volts.

Figure 19 shows one of telemetry logs taken from the flight test site and was extracted from mission planner software, and then it's converted to Google earth format to be displayed.

XII. Conclusion and Further Works

As for now, many of DRO points can be achieved. But some of them are still being pursued as improvement still goes further, especially for the avionics systems to extend the flight formation ability ([9]-[12]). There are still many home works to do, to test and validate many performance parameters, and also to improve current design to meet higher levels of performance.

References

[1] Raymer, Daniel P., "Aircraft Design: A Conceptual Approach", AIAA Education Series, Washington, US, 1989.

[2] Gabriel Staples. Electricrcaircraftguy. 2014. (Accessed on July 14th, 2015). VIEW

[3] Martin Hepperle. MH-Aerotools. 2002. (Accessed on July 14th, 2015). VIEW

[4] Aerovironment UAS: RQ-11B Raven Tech Spec document. (Accessed on july 14th, 2015). VIEW

[5] Aerovironment UAS: Wasp AE tech spec document. (Accessed on July 14th, 2015). VIEW

[6] Hadi, G., Varianto, R., Trilaksono, B., & Budiyono, A., "Autonomous UAV System Development for Payload Dropping Mission", Journal of Instrumentation, Automation and Systems, 1(2), 2014, pp. 72–77.

[7] Higashino, S., & Funaki, M., "Development and Flights of Ant-Plane UAVs for Aerial Filming and Geomagnetic Survey in Antarctica", Journal of Unmanned System Technology, vol. 1(2), 2013, pp. 37– 42.

[8] Mohammad H. Sadraey, "Optimal control and line-of-sight guidance formation flight", International Journal of Intelligent Unmanned Systems, vol. 1(3), 2013, pp.228–244. CrossRef

[9] Takuma Hino, Takeshi Tsuchiya, "Heuristic path planning of unmanned aerial vehicle formations", International Journal of Intelligent Unmanned Systems, vol. 1(2), 2013, pp.12 –144.

[10] Haoyang Cheng, John Page, John Olsen, "Cooperative control of UAV swarm via information measures", International Journal of Intelligent Unmanned Systems, vol. 1(3), 2013, pp.256–275. CrossRef

[11] Yi-Ren Ding, Yi-Chung Liu, Fei-Bin Hsiao, "The application of extended Kalman filtering to autonomous formation flight of small UAV system", International Journal of Intelligent Unmanned Systems, vol. 1(2), 2013, pp.154–186. CrossRef

[12] Brenton K. Wilburn, Mario G. Perhinschi, Hever Moncayo, Ondrej Karas, Jennifer N. Wilburn, "Unmanned aerial vehicle trajectory tracking algorithm comparison", International Journal of Intelligent Unmanned Systems, vol. 1(3), 2013, pp.276–302. CrossRef

[13] Ghassan Al-Sinbol, Mario G Perhinschi, Brenton K Wilburn, "Simplified GPS model for UAV fault tolerant control laws design", International Journal of Intelligent Unmanned Systems, vol. 3(1), 2015, pp.39–60. CrossRef

[14] Sanketh Ailneni, Sudesh K. Kashyap, N. Shantha Kumar, "INS/GPS fusion architectures for unmanned aerial vehicles", International Journal of Intelligent Unmanned Systems, vol. 2(3), 2014, pp.154–167. CrossRef

[15] Pessanha Santos, N., Melício, F., Lobo, V., & Bernardino, A., "A Ground-Based Vision System for UAV Pose Estimation", International Journal of Robotics and Mechatronics, vol. 1(4), 2014, pp. 138–144.

[16] Bottyan, Z., Wantuch, F., & Gyöngyösi, Z., "Forecasting of Hazardous Weather Phenomena in a Complex Meteorological Support System for UAVs", Journal of Unmanned System Technology, vol. 2(2), 2014, pp. 79–86.

[17] Iwata, K., "Research of Cargo UAV for civil transportation", Journal of Unmanned System Technology, vol. 1(3), 2013, pp. 89–93.

[18] XFLR5 Documentation Page. 2015. VIEW